# X-ray-line polarization spectroscopy in laser-produced plasmas

J. C. Kieffer, J. P. Matte, M. Chaker, and Y. Beaudoin
*Institut National de la Recherche Scientifique—Énergie et Matériaux, Case Postale 1020, Varennes, Québec, Canada H3X 1S2*

C. Y. Chien, S. Coe, and G. Mourou
*Center for Ultrafast Optical Science, University of Michigan, Ann Arbor, Michigan 48109-2099*

J. Dubau
*Observatoire de Paris, Centre National de la Recherche Scientifique, Département d'Astrophysique Relativiste et de Cosmologie, 92195 Meudon, France*

M. K. Inal
*Institut des Sciences Exactes, Boite Postale 119, 13000 Tlemcen, Algeria*
(Received 1 July 1993)

In this work, we show that x-ray-line polarization spectroscopy can be a powerful diagnostic to study laser-produced plasmas. Kinetic calculations are compared to experiments designed to probe the low-density plasma region (with a 1-ps laser pulse) and the overdense plasma (with a 400-fs laser pulse). We observe the transition from a "pancakelike" electron distribution function at low density to a "beamlike" electron distribution function in the overdense plasma. The results are in agreement with the calculations which indicate non-Maxwellian behavior and strong anisotropy due to nonlocal electron heat flow.

PACS number(s): 52.40.Nk, 52.25.Fi, 52.25.Nr, 52.70.La

## I. INTRODUCTION

The problem of the energy transport in a laser-produced plasma has received considerable attention in the past years. The classical linear thermal conduction formula of Spitzer and Härm [1] and Braginskii [2] is based on a first-order Chapman-Enskog perturbation calculation, and is valid only when the temperature gradient length is very much longer than the electron mean free path [3]. A unique problem associated with laser-produced plasmas are the rapid and extreme spatial and temporal gradients. In these plasmas Fourier's law breaks down and an *ad hoc* solution to this problem has long been to use so-called flux limiters in hydrodynamic codes [4]. However, a quantitative understanding of laser-produced plasmas, in view of several important applications including inertial confinement fusion [5], x-ray lasing [6], and laser plasma x-ray sources [7,8], requires kinetic modeling [9,10].

Simulations [9–15] of the transport in steep temperature gradient indicate that the heating of the plasma results in a nonlocal electron heat flow, from the underdense hot plasma into the cold dense plasma, supported mainly by electrons with large velocities (about three times the thermal velocity). The high-energy part of the electron velocity distribution exhibits noticeable deviations from a Maxwellian behavior; this effect can have important consequences. For example, in laser fusion, these electrons can preheat the D-T fuel thus preventing effective compression [16]. The delocalization model [17–19], which emerges from these studies, has provided a means of modeling the preheating phenomena in hydrodynamic codes, but does not include the deformation of the electron distribution due to the nonlocal transport and to the inverse bremsstrahlung absorption [20] which can significantly affect the ionization and excitation rates [21] and hence the dynamics of laser x-ray sources.

In this paper we present and discuss the method of x-ray-line polarization spectroscopy which gives the possibility to experimentally address the transport issue in laser-produced plasmas and allows also to test the predictions of kinetic codes. For the calculations the electron distribution function is expanded in Legendre polynomials. The heat flow is proportional to a moment of the first-order anisotropy $f_1$ of the electron distribution function due to the gradient of the isotropic component $f_0$. The gradients of the fluxes $f_1$ induce a second-order anisotropy $f_2$ of the electron distribution function. Calculations [22] predict a depletion of electrons with large axial velocities in the energy deposition zone resulting in a strong *negative* second-order anisotropy $f_2$ near the critical density $n_c$ which is equivalent to the oblate distribution function shape, in velocity space, in this region. On the other hand, a surplus of these electrons appears in the cold dense plasma, giving far from $n_c$ and near the target surface a *positive* but weaker anisotropy $f_2$ (beamlike electron velocity distribution function). $f_2$ and higher-order anisotropies usually have a negligible effect on the heat transport in-plane geometry [9,11] and are usually neglected in transport modeling [10,14]. In fact, a second-order anisotropy has been studied mostly because it can drive the Weibel instability [22–24]. However, another very interesting aspect is that $f_2$ gives a way to experimentally address the transport problem and test numerical predictions [25]. Indeed when ions are excited by collisions with electrons whose velocity distribution is

 

anisotropic, the resulting line emission is polarized [26]. In the following we discuss the application of the x-ray-line polarization spectroscopy to laser-produced plasmas.

In Sec. II we present the general characteristics of the line polarization. In Sec. III, we discuss the application of the diagnostic to laser-produced plasmas. Calculated polarizations for He-like and Li-like emissions are compared to experimental results obtained with an Al plasma produced by an ultrashort pulse in Sec. IV. We also discuss the interests and the limitations of such a diagnostic. We summarize in Sec. V.

## II. X-RAY-LINE POLARIZATION

When ions are excited by collisions with electrons whose velocity distribution is anisotropic, the resulting emission lines are partially polarized [26–29]. The fundamental asymmetry in the problem is in the orbital motion of the colliding electrons. Taking the direction of spatial gradients as the axis of reference for the quantization of angular momentum, it can be shown [26–29] that some magnetic sublevels are preferentially populated giving rise to significant linear polarization $P$ for the radiation emitted during the decay of these sublevels. This polarization diagnostic has already been used in the x-ray range [30–33] (for solar flares) and also in the x-uv range [34]. This diagnostic is complementary to the continuum polarization diagnostic which is effective for higher-energy electrons [35].

### A. Dependence of $P$ on velocity distribution anisotropy

When the velocity of electrons is azimuthally symmetric with respect to a given axis $z$, the polarization of the radiation resulting from impact excitation of ions by electrons can be readily calculated. Given a monoenergetic electron population with pitch angle distribution $f(\alpha)$, where $\alpha$ is the angle between the velocity and the $z$ axis, the photons emitted at an angle $\theta$ from the $z$ axis have a polarization

$$P(\theta)=Q(\theta)/I(\theta) ,$$

where $I(\theta)$ and $Q(\theta)$ are, respectively, given by expressions (11a) and (12a) from Ref. 33:

$$I(\theta)=\frac{3I_0}{4(3-P_0)}\int_0^{\pi}[2-P_0(2\cos^2\alpha\cos^2\theta+\sin^2\alpha\sin^2\theta)]f(\alpha)\sin\alpha\, d\alpha , \quad (1)$$

$$Q(\theta)=\frac{3I_0P_0}{4(3-P_0)}\sin^2\theta\int_0^{\pi}(3\cos^2\alpha-1)f(\alpha)\sin\alpha\, d\alpha . \quad (2)$$

Averaging over the azimuthal angle about $z$ axis has been assumed. Furthermore, the pitch angle distribution is normalized according to

$$2\pi\int_0^{\pi}f(\alpha)\sin\alpha\, d\alpha=1 .$$

$P_0$ is the polarization of photons, observed at right angle ($\theta=\pi/2$) to a monoenergetic electron beam incident along the $z$ axis. $I_0$ is the total intensity integrated over all observation angles.

Let us expand the pitch angle distribution in Legendre polynomials,

$$f(\alpha)=f_0+\sum_{l=1}^{N}f_lP_l(\mu)$$

with

$$f_l=\frac{2l+1}{2}\int_{-1}^{1}f(\alpha)P_l(\mu)d\mu ,$$

where $\mu=\cos\alpha$. Then, this gives us for (1) and (2)

$$I(\theta)=I_0\left[f_0+\frac{P_0f_2}{5(3-P_0)}(1-3\cos^2\theta)\right] , \quad (3)$$

$$Q(\theta)=\frac{3I_0P_0f_2}{5(3-P_0)}\sin^2\theta , \quad (4)$$

and the polarization is

$$P(\theta)=\frac{3P_0(f_2/f_0)\sin^2\theta}{5(3-P_0)+P_0(f_2/f_0)(1-\cos^2\theta)} . \quad (5)$$

Only two terms ($f_0$ and $f_2$) affect the line polarization and the angular distribution (contrary to bremsstrahlung the line emission angular distribution is not influenced by the fluxes $f_1$). In particular, for a beam incident along the $z$ axis we have $f(\alpha)=\delta(\cos\alpha-1)$, which gives $f_0=\frac{1}{2}$, $f_2=\frac{5}{2}$, and $P(\pi/2)=P_0$. If all the electrons have only radial velocities we have an infinitely thin pancake distribution in velocity space and $f(\mu)=\delta(\mu)$ which gives $f_0=\frac{1}{2}$, $f_2=-\frac{5}{4}$, and $P(\pi/2)=-P_0/(2-P_0)$. Figure 1 shows the variation of the polarization as a function of the anisotropy factor $f_2/f_0$ for an observation at 90° from the $z$ axis, which will be identified to the laser incidence axis (normal to the target surface), and for $P_0=0.6$. For solar flares, Haug (Ref. 33) used a convenient expression for the pitch angle distribution which is $f(\alpha)=(n+1)/2\pi\cos^n\alpha$ for $0\le\alpha\le\pi/2$. In these conditions $f_0=1/4\pi$, $f_2=(5/8\pi)[2n/(n+3)]$, and from expression (5), $P(\pi/2)=nP_0/(n+3-P_0)$ which is the

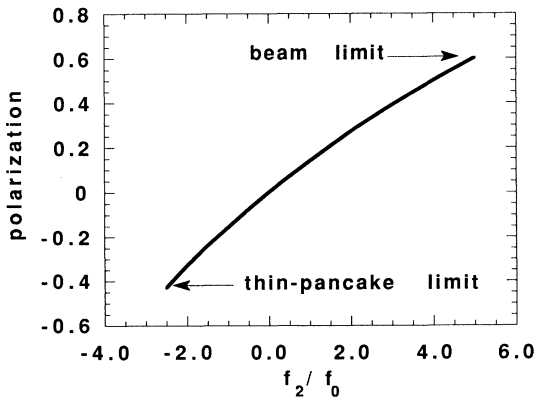


FIG. 1. Polarization as a function of the anisotropy factor $f_2/f_0$ [expression (5)] for observations at 90° from the laser incidence axis. These calculations have been done with $P_0=0.6$.

result obtained in Ref. 33 from direct integration.

In most cases, the incident electrons have an energy distribution $F(E)$. Then the line polarization is

$$P=\frac{\int_{E_{\rm th}}^{\infty} Q(\theta,E)F(E)dE}{\int_{E_{\rm th}}^{\infty} I(\theta,E)F(E)dE}\ , \tag{6}$$

where $E_{\rm th}$ is the threshold energy required for the excitation of the line considered. Now to carry this calculation we have to evaluate the behavior of the total intensity $I_0(E)$ of the polarization at right angles from the electron's beam axis $P_0(E)$ and of the isotropic and anisotropic factors, respectively, $f_0(E)$ and $f_2(E)$, with the electron energy $E$.

### B. Polarization $P_0$ for aluminum

The linear polarization of various lines emitted by Li-like and He-like ions has been already calculated [28,29,36,37] for higher-$Z$ elements which are of interest for astrophysical plasmas. However, in laser-produced plasmas, the electron temperature near the critical density is several hundred eV. Then the group of electrons which are responsible for the heat transfer have energies of a few keV. To probe the anisotropy of this group of electrons the emission line, whose polarization is considered, has to be matched to the electron energy. This requires the use of lower-$Z$ elements. We have chosen to study the polarization of aluminum $He_\alpha$ resonance and intercombination lines and of Li-like satellites. These lines are usually important for density and temperature diagnostics [38,39]. They allow the study of 2-keV electrons and, as Al has an $I=\frac{5}{2}$ nuclear spin, the intercombination line, which is expected to be practically unpolarized due to hyperfine interactions [36], can be used to compare the detection efficiency for both polarizations. The resonance line and the satellites which may be produced at different densities can also allow the probing of the electron distribution at various positions inside the density gradient. Finally, these lines are suitable for a simple and compact detection geometry with a Johann spectrometer used as a Bragg polarimeter.

#### *1. He- and Li-like lines*

The polarizations of He- and Li-like aluminum lines emitted by electron beams have been evaluated by two of us (J.D. and M.K.I.) with the method developed and presented in Refs. 28 and 29 which does not include hyperfine structure level separation. The populations of magnetic sublevels of $He_\alpha$ lines and of inner shell satellites, respectively, in Gabriel notations [40], the resonance $w$ ($1s^2-1s2p\ ^1P_1$), intercombination $y$ ($1s^2-1s2p\ ^3P_1$), and satellites $q$ [$1s^22s-1s2p(^1P)2s\ ^2P_{3/2}$], $s$ [$1s^22s-1s2p(^3P)2s\ ^2P_{3/2}$], and $u$ ($1s^22s-1s2s2p\ ^4P_{3/2}$), have been calculated assuming that direct electron-impact excitation from the ground state is the dominant populating mechanism. The degree of linear polarization at right angle from the incident electron beam is for the $w$ and $y$ lines

$$P_0=\frac{\Omega_0-\Omega_1}{\Omega_0+\Omega_1}\ , \tag{7}$$

where the $\Omega_i$'s are the collision strengths, the subscript $i$ designating the value of the projection $|M_i|$ of the angular momentum $J_i=1$. The collision strengths for transitions from the $1s^2\ ^1S_0$ ground level to the $1s2p\ ^{1,3}P_1$ levels and their individual magnetic sublevels $M_i$ in He-like Al XII ion are given in Table I. The variation of the linear polarization degree, calculated for the Al $w$ line, as a function of the energy of the electron beam is shown in Fig. 2(a). Near the excitation threshold the polarization $P_0$ [which is defined by $P_0=(I_\parallel-I_\perp)/(I_\parallel+I_\perp)$ where $I_\parallel$ ($I_\perp$) is the intensity of emitted photons having a polarization vector parallel (perpendicular) to the incident beam axis] is positive (+60%) for the $w$ line. It is interesting to note that the $w$ line polarization degree, plotted as a function of the electron energy in threshold units is almost independent of nuclear charge, as shown in Fig. 2(b) (polarization of the Al and Fe $w$ lines) and as observed in recent calculations [41].

Figure 3 presents the polarization degree calculated as a function of the energy of the beam $E$, the observation angle being at $\pi/2$ from the beam axis, for the satellites $q$, $s$, and $u$ whose upper levels are populated by inner-shell excitation. From Figs. 2(a) and 3, we see that the ratio $q/w$, which is proportional to the Li- to He-like ion abundance for an isotropic electron distribution [28,42], decreases slightly from 0.6 to 0.5 when $E$ increases as already obtained with Fe calculations. It is worthwhile to note in passing that the polarizations of the Al $q$ line are close to the Fe values for electron energies in threshold units. On the other hand, the $P_0$ values for the two inter-

TABLE I. Collision strengths for transitions from the $1s^2\ ^1S_0$ ground state to the $1s2p\ ^{1,3}P_1$ levels and their magnetic sublevels $M_i$. The threshold energies $\Delta E$ and the electron-impact energies $k_j^2$ are in rydbergs. The last line for each state corresponds to the total collision strength ($\Omega_T=\Omega_0+2\Omega_1$). The numbers in square brackets denote powers of 10.

| | | | $k_j^2$ (Ry) | | | | |
|---|---|---|---|---|---|---|---|
| State | $M_i$ | $\Delta E$ (Ry) | 120 | 180 | 250 | 500 | 800 |
| $1s2p\ ^3P_1$ | 0 | | 4.03[−4] | 2.15[−4] | 1.44[−4] | 8.53[−5] | 7.12[−5] |
| | 1 | | 1.19[−3] | 6.21[−4] | 3.47[−4] | 1.04[−4] | 6.30[−5] |
| | $\Omega_0+2\Omega_1$ | 116.67 | 2.79[−3] | 1.46[−3] | 8.38[−4] | 2.94[−4] | 1.97[−4] |
| $1s2p\ ^1P_1$ | 0 | | 5.40[−3] | 1.07[−2] | 1.48[−2] | 2.105[−2] | 2.35[−2] |
| | 1 | | 1.39[−3] | 2.76[−3] | 4.51[−3] | 1.02[−2] | 1.52[−2] |
| | $\Omega_0+2\Omega_1$ | 117.46 | 8.18[−3] | 1.63[−2] | 2.38[−2] | 4.14[−2] | 5.39[−2] |

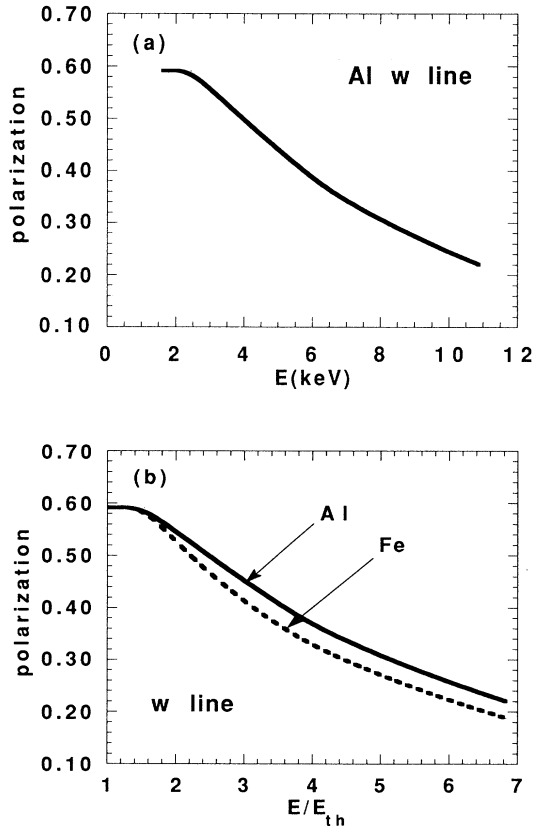


FIG. 2. Linear polarization degree $P_0$ calculated (a) for the Al $w$ line as a function of the electron energy; (b) for Al and Fe $w$ lines as a function of the electron energy in threshold units.

combination transitions $y$ and $u$ have similar behaviors with the electron energy and are very different from the higher $Z$ values [28,36].

### 2. *Effect of the hyperfine interaction*

As already mentioned, Al has an $I=\frac{5}{2}$ nuclear spin. Its nuclear $g$ factor [43] is $g_I=1.457$. In Al XII ions the hyperfine structure of the $^1P_1$ level is very small compared to its radiative width. The situation is different for the $^3P_1$ level which has a radiative width of about $4.8\times10^{-5}$ eV while the calculated energy splitting between consecutive hyperfine components $F$ and $F-1$ is $3.14\times10^{-3}$ eV for $F=\frac{7}{2}$ and $2.24\times10^{-3}$ eV for $F=\frac{5}{2}$.

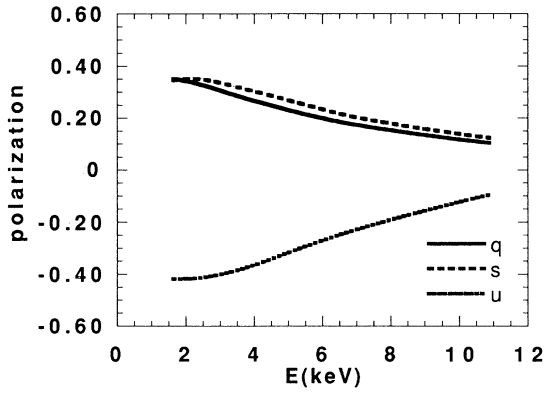


FIG. 3. Polarization fraction $P_0$ calculated for the inner-shell excited satellites $q$, $s$, and $u$ (Li-like Al).

Then, while the hyperfine interaction does not affect the polarization of the line $w$, it has a strong depolarization effect on the line $y$. This depolarization effect can be taken into account by using the method of state multipoles and perturbation coefficients described, for instance, in Ref. 44. Then, the degree of polarization of the line $y$ (in the presence of hyperfine structure which is almost fully resolved) becomes

$$P_0=\frac{3G_2(\Omega_0-\Omega_1)}{(2+G_2)\Omega_0+(4-G_2)\Omega_1}\ , \tag{8}$$

where the perturbation coefficient $G_2$ is given by

$$G_2=\frac{1}{2I+1}\sum_F(2F+1)^2\begin{Bmatrix}1 & F & I\\ F & 1 & 2\end{Bmatrix}^2\ , \tag{9}$$

$\{\ \}$ being a $6j$ symbol. For Al ($I=\frac{5}{2}$) we have $G_2=0.2216$.

The line $y$ is blended with the line arising from the decay of the $^3P_0$ level to the $^1S_0$ ground level via a hyperfine induced $E1$ transition. To take this $^1S_0$-$^3P_0$ transition, which is unpolarized, into account one has to add the product $2R\,\Omega(^3P_0)$ in the denominator of Eq. (8). $\Omega(^3P_0)$ is the collision strength for the $^1S_0\rightarrow{}^3P_0$ excitation and $R$ is the branching ratio for the $^3P_0\rightarrow{}^1S_0$ radiative decay. The calculated radiative rates from the $^3P_0$ state are $A(^3P_0\rightarrow{}^3S_1)=1.34\times10^8\ \mathrm{s}^{-1}$ and $A(^3P_0\rightarrow{}^1S_0)=6.6\times10^7\ \mathrm{s}^{-1}$ which gives $R=0.33$, in good agreement with the Mohr calculations [45] ($R=0.35$). Our calculations of the $^3P_0\rightarrow{}^1S_0$ radiative rate have been carried out in the first-order perturbation approximation. Only the magnetic dipole hyperfine interaction was considered, i.e., electric quadrupole effects were neglected. The required matrix elements of the dipole hyperfine operator between the $^3P_0$ state and the $^3P_1$ $F=\frac{5}{2}$ and $^1P_1$ $F=\frac{5}{2}$ states have been computed using hydrogenic wave functions. The $^3P_0$-$^3P_1$ fine-structure splitting and the $^3P_0$-$^1P_1$ energy difference were taken from the refined calculations of Drake [46].

Figure 4 shows the depolarization effect of the $y$ line due to the hyperfine interaction. It is clearly seen that the polarization degree is strongly reduced to less than 9% near the threshold. We expect similar depolarization effects on $u$ and maybe on $s$ lines. The present calculations could be improved by taking into account (i) the stark broadening effects which could eventually slightly increase the polarization of the $y$ line, and (ii) the quenching of the $1s2s\ ^1S_0$ level by high microfields which produces a new line, blended to the $y$ line and which is unpolarized, therefore increasing the depolarization effect of the $y$ line [47].

### C. Total intensity $I_0$

The total intensity $I_0(E)$ is proportional to the impact excitation cross section $\sigma(E)$. We have

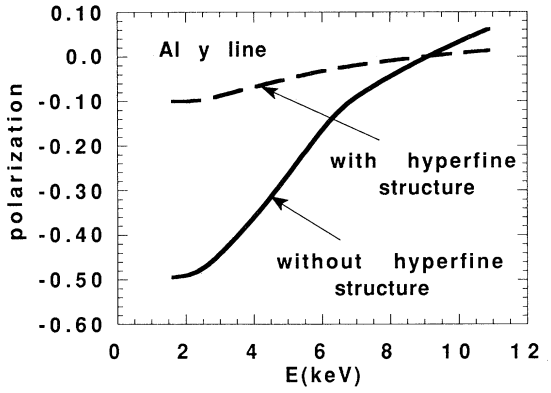


FIG. 4. Polarization fraction $P_0$ calculated for the Al $y$ line with and without the effect of hyperfine structure.

$$I_0(E) \sim \sqrt{E}\,\sigma(E)$$

with $\sigma(E)=\Omega(^1P)/\varepsilon$ where $\varepsilon$ denotes the electron-impact energy in threshold units and where $\Omega(^1P)$ is the collision strength given in Table I.

## III. APPLICATION TO LASER-PRODUCED PLASMAS

In laser-produced plasmas the nonlocal transport and the inverse bremsstrahlung absorption produce a strongly non-Maxwellian electron distribution. Furthermore, the gradients of the fluxes induce a second-order anisotropy of the electron distribution function $f_2$. Then, a measurement of the polarization of x-ray lines from ions collisionally excited by non-Maxwellian, anisotropic electron distribution will provide insight into the electron kinetic behavior of the plasma [25]. Anisotropy probing ideally requires an emission strongly localized at a given electron density. One-dimensional (1D) Lagrangian simulations [48] indicate that this can be obtained with an ultrashort laser pulse (picosecond or subpicosecond pulse) incident on a low-temperature preformed plasma having an extension of a few microns. In laser-produced plasmas the anisotropy factor $f_2/f_0$ varies in a complex way with the electron energy and with the electron density. We use electron kinetic calculations to evaluate the isotropic part $f_0$ of the electron distribution and the second-order anisotropy $f_2$. Then, line polarization is deduced for various conditions from the $f_2/f_0$ curves taking into account the variation of $P_0$ with the electron energy.

Our electron kinetic code FPI has been presented previously [15,22] so we will discuss it only very briefly here. The code computes the evolution of the electron velocity distribution function in a plasma heated by inverse bremsstrahlung absorption of laser radiation. Propagation and absorption of the normally incident laser beam, electron transport under the influence of spatial gradients and of the ambipolar field, hydrodynamic expansion, and a simplified model for atomic physics, which includes both ionization from the ground state, and excitation are included. The code is one dimensional in space, but two dimensional in velocity space; the velocity distribution is assumed to be azimuthally symmetric, and the pitch angle distribution is expanded in Legendre polynomials. In the code, it is the coefficients of this Legendre expansion which are advanced in time. Diagnostics such as $He_\alpha$ emission and its polarization are done in a post-processing mode.

We have performed electron kinetic simulations on an ultrashort pulse interacting with a preformed low-temperature plasma. Calculations have been done for 400-fs and 1-ps pulses (1-$\mu$m wavelength) incident at intensities ranging from $10^{14}$ to $10^{16}$ W/cm$^2$ on a preformed plasma having an exponential density profile with initial gradients scale lengths of 1, 4, and 10 $\mu$m. These condi-

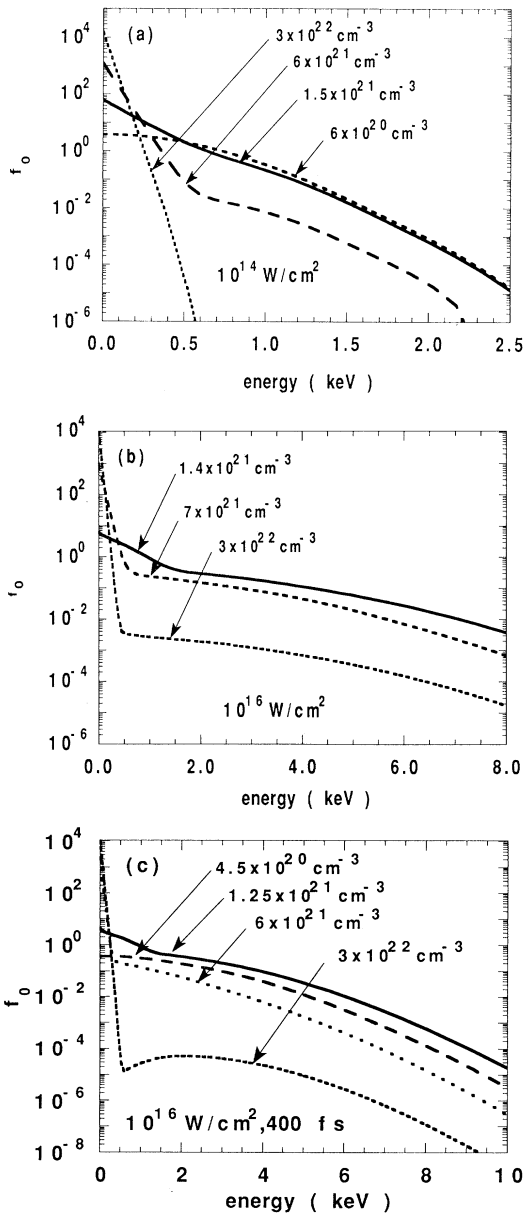


FIG. 5. Isotropic part $f_0$ of the electron distribution calculated at the peak of the main pulse for an initial gradient scale length $L=1$ $\mu$m. (a) 1-ps pulse at $10^{14}$ W/cm$^2$; (b) 1-ps pulse at $10^{16}$ W/cm$^2$; (c) 400-fs pulse at $10^{16}$ W/cm$^2$.

tions are relevant to those of our experiments [25] in which we try to produce the shortest line emission [49] localized in a very narrow density range (adjusted by changing the pulse length and the prepulse). Calculations have been realized on a time scale of a few picoseconds.

### A. Isotropic part $f_0$

Figure 5 shows the isotropic part $f_0$ of the electron distribution calculated at the *peak* of the main short pulse and at different positions (and densities) in the density gradient, for an initial gradient scale length $L=1$ $\mu$m. Comparison of Fig. 5(a) (1-ps pulse at $10^{14}$ W/cm$^2$) and Fig. 5(b) (1-ps pulse at $10^{16}$ W/cm$^2$) indicates that the electron distribution $f_0$ exhibits a strong departure from the Maxwellian shape particularly in the dense plasma and at higher intensity. The electron distribution shape is not strongly dependent on the short pulse duration as we can see by comparing Fig. 5(b) (1-ps pulse at $10^{16}$ W/cm$^2$) and Fig. 5(c) (400-fs pulse at $10^{16}$ W/cm$^2$). In the colder parts of the heat front there is a surplus of hot electrons which occurs because the more energetic electrons stream from the hot plasma into the cold plasma on a time shorter than the time taken by electron-electron collisions to establish an equilibrium with the local population. It is these electrons which excite Li-like satellite lines in the cold plasma. This non-Maxwellian effect which is a manifestation of nonlocal transport has to be taken into account for a quantitative understanding of ultrafast x-ray sources [49].

### B. Second-order anisotropy

Figure 6 shows the second-order anisotropy $f_2/f_0$ calculated at the peak of the main pulse, at different positions in the plasma, for an initial gradient scale length $L=1$ $\mu$m, for a 1-ps pulse at $10^{14}$ W/cm$^2$ [Fig. 6(a)] and at $10^{16}$ W/cm$^2$ [Fig. 6(b)] and for a shorter pulse (400 fs) at $10^{16}$ W/cm$^2$ [Fig. 6(c)]. In all the cases we observe a strong negative second-order anisotropy in the underdense plasma. The minimum anisotropy value ($f_2/f_0 \simeq -1$) appears at an electron energy which is greater with higher intensity or longer pulse. This anisotropy is the result of a depletion of electrons with large axial velocities in the corona and in the energy deposition zone resulting in an oblate distribution function shape (pancakelike). As the density increases the anisotropy increases and becomes positive in the very dense plasma, which corresponds to a prolate distribution function shape (beamlike).

The negative anisotropy in the underdense plasma is reduced and even suppressed as the initial gradient scale

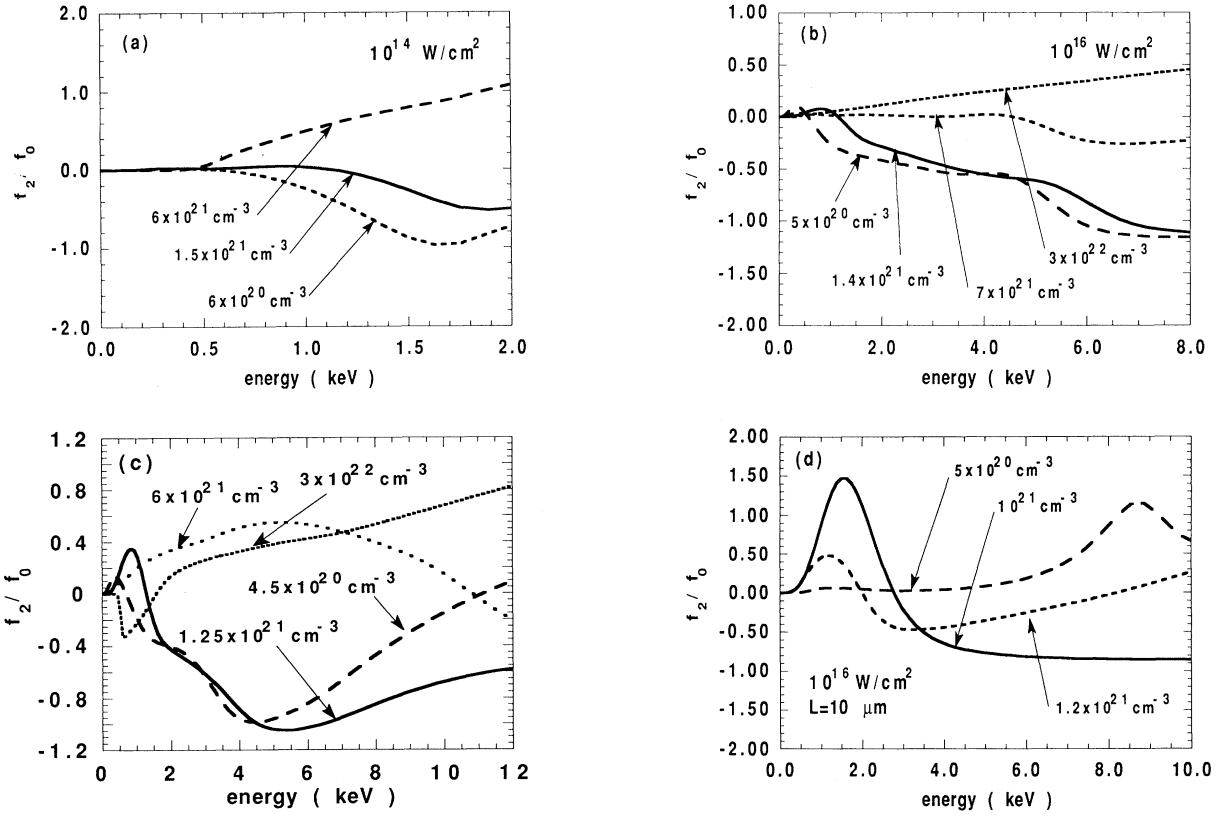


FIG. 6. Second-order anisotropy $f_2/f_0$ calculated at the peak of the main pulse for (a) a 1-ps pulse incident at $10^{14}$ W/cm$^2$ on an initial gradient scale length $L=1$ $\mu$m; (b) a 1-ps pulse incident at $10^{16}$ W/cm$^2$ on an initial gradient scale length $L=1$ $\mu$m; (c) a 400-fs pulse incident at $10^{16}$ W/cm$^2$ on an initial gradient scale length $L=1$ $\mu$m; (d) a 400-fs pulse incident at $10^{16}$ W/cm$^2$ on an initial gradient scale length $L=10$ $\mu$m.

length $L$ is increased as can be noted by comparing the results obtained for a 400-fs pulse incident at $10^{16}$ W/cm$^2$ on a gradient scale length of $L=1$ $\mu$m [Fig. 6(c)] and $L=10$ $\mu$m [Fig. 6(d)]. This indicates that the gradient scale length is a *crucial* parameter for the anisotropy and thus for the x-ray-line polarization.

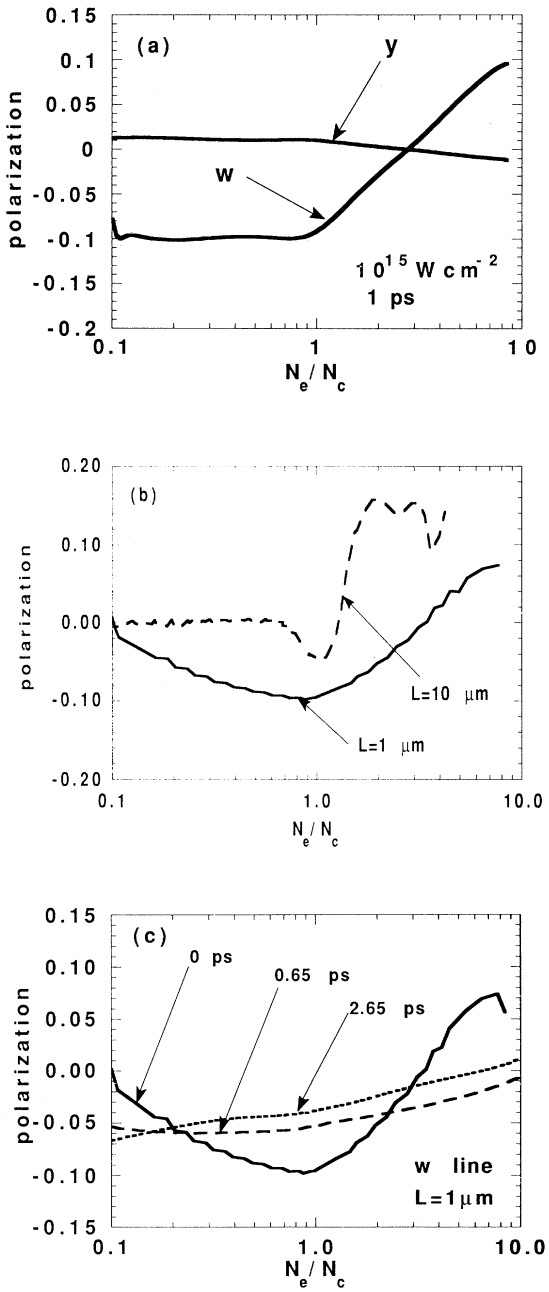


FIG. 7. He-like Al lines polarizations calculated as a function of the electron density $n/n_c$ [where $n_c$ is the critical density ($n_c \simeq 10^{21}$ cm$^{-3}$)]; (a) at the peak of the short pulse for a 1-ps pulse at $10^{15}$ W/cm$^2$, $L=1$ $\mu$m; (b) at the peak of the short pulse for a 400-fs pulse at $10^{16}$ W/cm$^2$, $L=1$ and 10 $\mu$m; (c) at different times after the peak of the short pulse (time 0 ps) for a 400-fs pulse at $10^{16}$ W/cm$^2$, $L=1$ $\mu$m.

### C. Polarization of He-like lines

We calculate the polarization that the $w$ (resonance) and $y$ (intercombination) Al lines would have, as a function of the density at which the emission takes place, due to the electron distribution previously described. The $y$ line is unpolarized as shown in Fig. 7(a) (1-ps pulse, $10^{15}$ W/cm$^2$, $L=1$ $\mu$m, peak of the pulse). A similar result is obtained for the $y$ line with different pulse lengths, different intensities, or different gradient scale lengths indicating that this line can be used with good confidence as a reference to monitor the diagnostic polarization efficiency. The $w$ line would have a negative polarization if produced in the underdense plasma. Figure 7 shows the polarization expected for the $w$ line in various conditions. The main point of these calculations is that the polarization of the $w$ line would be positive if the emission region is localized in the overdense plasma. If the He$_\alpha$ emission is produced in the underdense plasma, as observed in experiments realized with a 1-ps pulse [25], then the observation of the line polarization requires a low intensity and a short gradient scale length. The negative polarization in the underdense plasma is reduced as the gradient scale length is increased as shown in Fig. 7(b). A polarization $P=-0.18$ is calculated at $n=0.8n_c$ when a 1-ps pulse at $10^{14}$ W/cm$^2$ is incident on a gradient scale length $L=1$ $\mu$m.

Calculations show that the isotropic part $f_0$ and the second-order anisotropy retain their shape during a few picoseconds after the peak of the main pulse, without strong changes. Then the polarization relaxes only slowly with time as indicated in Fig. 7(c) (400-fs pulse at $10^{16}$ W/cm$^2$, $L=1$ $\mu$m). For these conditions nonstationary atomic physics modeling coupled to the Fokker-Planck code shows [50] that the peak of the He$_\alpha$ emission occurs 300 fs after the maximum of the laser pulse. Then, if the emission is produced on a sufficiently short time scale, at a few times the critical density, time integration effect will not be a problem for polarization measurements.

## IV. COMPARISON TO EXPERIMENTS

The experiments were carried out with the tabletop terawatt laser at the Center for Ultrafast Optical Science of the University of Michigan. Two different laser pulses have been used with different contrast ratios in order to produce an He$_\alpha$ emission at different densities. In this work we take advantage of the prepulse generated during the production and amplification of the short pulse (by the chirped-pulse amplification technique [51]) to produce a low-temperature preplasma. The disadvantage of this configuration is that the prepulse cannot be controlled independently of the short pulse, so the preplasma parameter cannot be separately adjusted. The advantage of the method is very good reproducibility in the preplasma formation and in the arrival time of the main pulse. This is very important because a large number of shots are required to obtain one spectrum.

In the first experiment [25] the laser was working with a glass regenerative amplifier. The 1-ps pulse (1.05 $\mu$m) was focused by an $f/7$ lens (in normal incidence) on

plane targets composed of 5000-Å-thick Al layer on a Si substrate. The intensity of the 1-ps pulse was about $8\times10^{14}$ W/cm$^2$, and the intensity of the 60-ps prepulse was about $8\times10^{11}$ W/cm$^2$. Our previous experiments indicate that such a prepulse produces a preplasma with a gradient scale length $L$ close to the laser wavelength [52,53]. The Al He$_\alpha$ line intensity ratios, measured at 45° from the laser axis with PET and RAP crystals (in Von Hamos or Johann configurations where polarization plays no role and should not be taken into account for the interpretation of resonance to intercombination line ratio), indicate [25] that the emission is mainly produced between $0.3n_c$ and $0.5n_c$ (where $n_c$ is the critical density). Fluid simulations [48] indicate that the prepulse alone produces a 100-eV preplasma with no significant He-like emission. Calculations also indicate that the He-like emission occurs mainly just after the 1-ps pulse, near $n_c$ and lasts a few picoseconds.

In the second, new, experiment the laser was working with a Ti:Sapphire regenerative amplifier [54]. The 400-fs pulse (1.05 $\mu$m) was focused by an $f/6$ spherical fused silica lens (in normal incidence) on plane targets composed of 5-$\mu$m-thick Al layer on a Si substrate (80-$\mu$m focal spot diameter). The intensity peak to background contrast ratio was measured, using a third-order autocorrelator, to be $5\times10^5$:1 at 1.053 $\mu$m. The intensity of the 400-fs pulse was about $10^{16}$ W/cm$^2$ and the intensity of the nanosecond long prepulse was about $2\times10^{10}$ W/cm$^2$. In these experimental conditions, the He$_\beta$ and the He$_\gamma$ line profiles indicate [49,55] (using Stark broadening modeling) that the He-like emission is radiated at a density of $2n_c$. A quantitative study of time-resolved spectra obtained with Al targets in the 8-Å range, with a 2-ps temporal resolution [49,56] indicates that the prepulse produces a gradient scale length of a few micrometers. The He$_\alpha$ resonance line has a 3-ps rise time and a relatively short duration [49,57] (a few picosecond full width at half maximum).

The polarization of the line radiation was measured with a Johann crystal spectrometer used as a Bragg polarimeter [31]. We used an ammonium dihydrogen phosphate crystal ($2d=10.64$ Å) with a 300-mm radius of curvature and a Bragg angle of 46.8°. The crystal (20×60 mm) center was at 220 mm from the Rowland circle. A diaphragm (10-mm diameter) was used at 70 mm from the crystal center to have the same crystal illumination in the two configurations, when the plasma is on the Rowland circle. The Al spectrum between 7.74 and 8 Å was observed in a direction nearly perpendicular (85°) to the laser incidence axis (normal to the target surface). Measurements were made at two crystal orientations which we call horizontal ($H$) and vertical ($V$) as schematically shown in Fig. 8. In the $H$ orientation the plane of dispersion of the crystal was horizontal, perpendicular to the target plane and radiation $I_\perp$ with the electric-field vector perpendicular to the laser incidence axis which was preferentially detected. To measure radiation $I_\parallel$ with the electric-field vector parallel to the laser incidence axis, the crystal was rotated by 90° around the line of sight.

The polarization efficiency of the spectrometer for the two crystal orientations has been calibrated with the $y$ (He$_\alpha$ intercombination) emission, which is unpolarized and optically thin. The plasma was on the Rowland circle to have the same crystal illumination in the two crystal configurations and also to avoid any changes in the source size when the spectrometer is rotated around the line of sight [25]. The observed $y$ line was unpolarized as expected. Figure 9(a) shows the $y$ line polarization measured in the low-density experiment (1-ps pulse). The experimental result is compared to calculation (at the peak of the pulse) for a 1-ps pulse incident at $10^{14}$ and $10^{15}$ W/cm$^2$ on a $L=1$ $\mu$m preplasma gradient scale length. The uncertainty on the data arises from laser intensity variations from shot to shot. However, these results indicate very similar parallel and perpendicular intercombination line intensities which means similar efficiencies for the two spectrometer orientations.

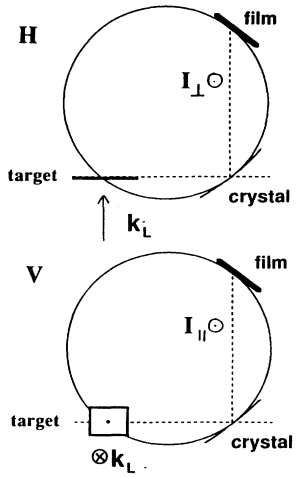


FIG. 8. Spectrometer orientations for polarization measurements. In the $H$ configuration, the plane of dispersion of the crystal is horizontal, perpendicular to the target plane. In the $V$ configuration, the plane of dispersion of the crystal is vertical, parallel to the target plane.

In the low-density experiment the $w$ line ($1s^2$-$1s2p$ $^1P$) has a negative polarization [25] ($P=-0.25\pm0.07$) due to the oblate or "pancakelike" distribution in the electron velocity space in the underdense plasma. The measured [25] (1-ps pulse) and calculated (1-ps pulse, $L/\lambda=1$, $10^{14}$ and $10^{15}$ W/cm$^2$) $w$ line polarizations appear in Fig. 9(b). The measurements indicate a greater anisotropy than the simulations. Using the calculated minimum anisotropy (1 ps, $10^{14}$ W/cm$^2$, $L/\lambda=1$) which is $f_2/f_0\simeq-1$ for 1.6 keV electrons at $6\times10^{20}$ cm$^{-3}$ [Fig. 6(a)], simple expression (5) gives a polarization $P(\pi/2)=-0.16$ as seen in Fig. 9(b). Then the measured $w$ line polarization roughly indicates [using expression (5)] an anisotropy $f_2/f_0\simeq-1.5$, which is greater than calculated but significantly lower than the thin pancake limit $f_2/f_0=-2.5$ (Fig. 1).

When the density at which the emission takes place increases, the He$_\alpha$ resonance line polarization tends towards positive values. The measured (400-fs pulse) and calculated (400-fs pulse at $10^{16}$ W/cm$^2$, $L/\lambda=1$) $w$ line

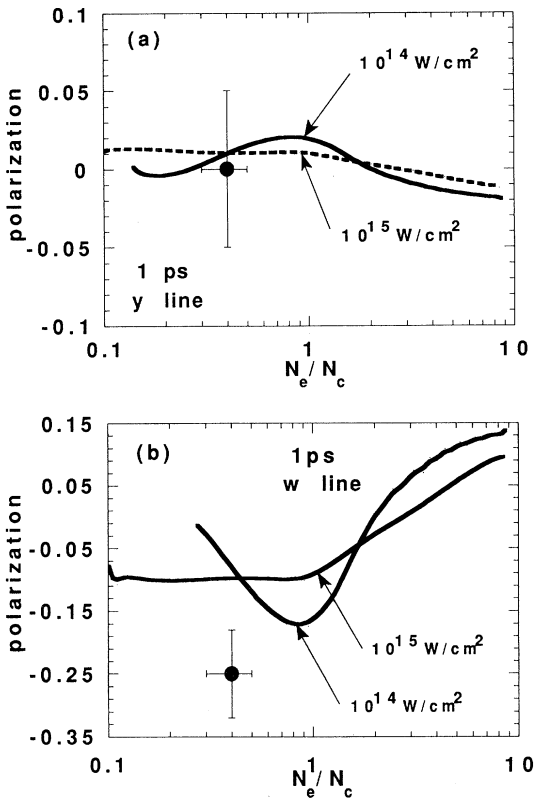


FIG. 9. Polarization measured (dots) and calculated (lines) for a 1-ps pulse as a function of the density at which the emission is produced. $n_c$ is the critical density ($10^{21}$ cm$^{-3}$). The experimental intensity is $8\times10^{14}$ W/cm.$^2$. Calculations have been done for $10^{14}$ W/cm$^2$ and $10^{15}$ W/cm$^2$ and with $L=1$ $\mu$m; (a) $y$ line; (b) $w$ line.

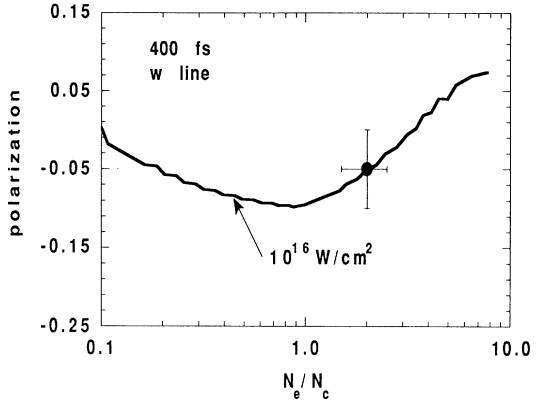


FIG. 10. Polarization of the Al $w$ line measured (dot) and calculated (line) for a 400-fs pulse as a function of the density at which the emission is produced. $n_c$ is the critical density ($10^{21}$ cm$^{-3}$). The experimental intensity is $10^{16}$ W/cm$^2$. Calculations have been done for $10^{16}$ W/cm$^2$ and $L=1$ $\mu$m.

polarizations appear in Fig. 10 for the high-density experiment and we see that we have a general agreement between the experiments and the calculations. The calculated polarization is not strongly sensitive to the laser intensity as already shown in Fig. 9(b). The mean polarization expected for 1-ps and 400-fs experiments were, respectively, about $-0.12$ and 0 while the observed polarizations are $-0.25\pm0.07$ and $-0.05\pm0.05$.

In the low-density experiments, the Li-like lines have greater parallel intensity [25] which could indicate either that the Li-like emission regions have radial dimensions larger than the axial size or that the Li-like emission has a positive polarization. The experiments with the shorter pulse confirm the previous observations. A positive polarization ($P=+0.08\pm0.07$) has been measured for the $q$, $r$ Li-like satellite. The polarization of these lines is expected to be positive because this emission has a positive $P_0$ (Fig. 3) and is produced in the overdense plasma where the electron distribution anisotropy is positive (beamlike shape in velocity space). However, in the absence of knowledge of the density at which this emission takes place, the Li-like results are less straightforward to interpret. It is worthwhile noting in passing that the time history [49] of the $a-d$, $q$, $r$ Li-like satellites (2-ps temporal resolution) can only be modeled [56] by taking into account the non-Maxwellian character of the electron distribution $f_0$ which indicate that these satellites are very sensitive to the nonlocal transport.

In this kind of plasma, two-dimensional (2D) effects might be important. However, the observation of similar $y$-line intensities in the two configurations and the observation of the same behavior with the plasma on the Rowland circle, where the emission zones are smaller, and inside the Rowland circle, tell us that 2D effects, if present, cannot really explain the measurements. The present calculations do not include any hot electrons such as those which could be radially produced by nonlinear processes at the surface of critical or quarter-critical densities [58–60]. The observation of $K\alpha$ emission in our experiment [57] could suggest the presence of a hot electron component which could eventually modify the polarization of the $He_\alpha$ radiation. The ion-acoustic turbulence is another effect which could increase the anisotropy of the electron distribution and strongly distort the electron distribution [61]. In this case the anisotropy of the turbulence spectrum induces an effect which depends on the polarization of the incident electromagnetic radiation. In the absence of ion-acoustic turbulence the oscillations of the electrons in the laser field will also enhance the anisotropy of the distribution [62] along the direction of the laser field. However, in our experimental conditions we do not observe any significant differences between polarization results obtained with $s$ (laser component along $I_\perp$) and $p$ (laser component perpendicular to both $I_\perp$ and $I_\parallel$) laser polarization. Finally, self-generated toroidal magnetic fields could have some effects, the perpendicular component $I_\perp$ being along the $B$ field while the parallel component $I_\parallel$ is perpendicular to the $B$ field.

## V. CONCLUSIONS

In summary, we show that x-ray-line polarization spectroscopy is a very powerful diagnostic for laser-produced

plasmas, to study nonlocal transport and have a direct access to the anisotropy of the electron distribution. The magnitude of the expected effect on the aluminum $He_\alpha$ ($1s^2$-$1s2p\ ^1P$) resonance emission is not very strong (polarization between $-0.15$ and $+0.15$ depending on the plasma density, gradient scale lengths, of the laser intensity) but is sufficiently large to be detected with a carefully designed experiment. By matching the plasma temperature, and the emission line, it is possible to use the technique to probe various ranges of electron energy along the density gradient. We compare calculations to experiments designed to probe the low-density plasma region (with a 1-ps laser pulse) and the overdense plasma (with a 400-fs laser pulse). We observe an increase of the $w$ line polarization as the density at which the emission takes place increases, in general agreement with the kinetic Fokker-Planck calculations which indicate a transition from a "pancakelike" electron distribution at low density to a "beamlike" distribution in the overdense plasma, related to the nonlocal electron heat flow in laser-produced plasmas.

## ACKNOWLEDGMENTS

The authors would like to thank T. W. Johnston and H. Pépin for their support and for many helpful discussions. We also thank C. Y. Côté for his help in data processing and C. Sirois for the technical support. One of us (J.C.K.) would like to thank P. Dhez and O. Peyrusse for many interesting discussions. This research was supported in part by the Ministère de l'Education du Québec and by Natural Sciences and Engineering Research Council of Canada.

[1] L. Spitzer and R. Härm, Phys. Rev. **89**, 977 (1953).
[2] J. I. Braginskii, in *Review of Plasma Physics,* edited by M. A. Leontovich (Consultants Bureau, New York, 1965), Vol. 1.
[3] D. R. Gray and J. D. Kilkenny, Plasma Phys. **22**, 81 (1980).
[4] R. C. Malone, R. L. McCrory, and R. L. Morse, Phys. Rev. Lett. **34**, 721 (1975).
[5] J. Nuckolls, L. Wood, A. Thiessen, and G. Zimmerman, Nature (London) **239**, 139 (1972); J. D. Lindl, in *Proceedings of the International Dawson Symposium on the Physics of Plasmas,* edited by T. Katsouleas (Addison-Wesley, Redwood City, CA, 1991), p. 177.
[6] D. L. Matthews *et al.*, Phys. Rev. Lett. **54**, 110 (1985); M. D. Rosen *et al.*, *ibid.* **54**, 106 (1985).
[7] K. M. Gilbert, J. P. Anthes, M. A. Gusinow, M. A. Palmer, R. R. Whitlock, and D. J. Nagel, J. Appl. Phys. **51**, 1449 (1980).
[8] M. M. Murnane, H. C. Kapteyn, and R. W. Falcone, Phys. Rev. Lett. **62**, 155 (1989).
[9] A. R. Bell, R. Evans, and D. J. Nicholas, Phys. Rev. Lett. **46**, 243 (1981).
[10] E. M. Epperlein, G. J. Rickard, and A. R. Bell, Phys. Rev. Lett. **61**, 2453 (1988).
[11] J. P. Matte and J. Virmont, Phys. Rev. Lett. **49**, 1936 (1982).
[12] R. J. Mason, Phys. Rev. Lett. **42**, 239 (1979).
[13] R. J. Mason, Phys. Rev. Lett. **47**, 652 (1981).
[14] J. R. Albritton, Phys. Rev. Lett. **50**, 2078 (1983).
[15] J. P. Matte, T. W. Johnston, J. Delettrez, and R. L. McCrory, Phys. Rev. Lett. **53**, 1461 (1984).
[16] A. Nishiguchi, K. Hima, H. Azechi, M. Miyanaga, and S. Nakai, Phys. Fluids B **4**, 417 (1992).
[17] J. F. Luciani, P. Mora, and J. Virmont, Phys. Rev. Lett. **51**, 1664 (1983).
[18] M. K. Prasad and D. S. Kershaw, Phys. Fluids B **3**, 3087 (1991).
[19] E. M. Epperlein and R. W. Short, Phys. Fluids B **3**, 3092 (1991).
[20] A. B. Langdon, Phys. Rev. Lett. **44**, 575 (1980).
[21] P. Alaterre, J. P. Matte, and M. Lamoureux, Phys. Rev. A **34**, 1578 (1986).
[22] J. P. Matte, A. Bendib, and J. F. Luciani, Phys. Rev. Lett. **58**, 2067 (1987).
[23] A. Ramani and G. Laval, Phys. Fluids **21**, 980 (1978).
[24] T. Okada, T. Yabe, and K. Niu, J. Phys. Soc. Jpn. **43**, 1042 (1977).
[25] J. C. Kieffer, J. P. Matte, H. Pépin, M. Chaker, Y. Beaudoin, C. Y. Chien, S. Coe, G. Mourou, and J. Dubau, Phys. Rev. Lett. **68**, 480 (1992).
[26] J. R. Oppenheimer, Z. Phys. **43**, 27 (1927).
[27] I. C. Percival and M. J. Seaton, Philos. Trans. R. Soc. London **251**, 113 (1958).
[28] M. K. Inal and J. Dubau, J. Phys. B **20**, 4221 (1987).
[29] M. K. Inal and J. Dubau, J. Phys. B **22**, 3329 (1989).
[30] I. A. Zhitnik, V. V. Korneev, V. V. Krutov, S. N. Oparin, and A. M. Ubnov, in *X-ray Spectroscopy and the Properties of Multiply-Charged Ions,* Proceedings of the Lebedev Physics Institute, edited by I. E. Sobelman (Nova Science, Commack, N.Y., 1988), Vol. 179, p. 51.
[31] R. Novick, Space Sci. Rev. **18**, 389 (1975).
[32] K. Akita, Solar Phys. **86**, 101 (1983).
[33] E. Haug, Solar Phys. **71**, 77 (1981).
[34] P. Dhez, Nucl. Instrum. Methods Phys. Res. A **261**, 66 (1987).
[35] M. Lamoureux, L. Jacquet, and R. H. Pratt, Phys. Rev. A **39**, 6323 (1989).
[36] J. R. Henderson, P. Beierdorfer, C. Bennett, S. Chantrenne, D. Knapp, R. E. Marrs, M. B. Schneider, K. L. Wong, G. Doschek, J. F. Seeley, C. M. Brown, R. E. LaVilla, J. Dubau, and M. A. Levine, Phys. Rev. Lett. **65**, 705 (1990).
[37] H. L. Zhang, D. H. Sampson, and R. E. H. Clark, Phys. Rev. A **41**, 198 (1990).
[38] H. J. Kunze, A. M. Gabriel, and H. R. Griem, Phys. Rev. **165**, 267 (1968).
[39] E. V. Aglitskii, V. A. Boiko, A. V. Vinogradov, and E. A. Yukov, Kvan. Elektron. (Moscow) **1**, 579 (1974) [Sov. J. Quantum Electron. **4**, 322 (1974)].
[40] A. H. Gabriel, Mon. Not. R. Astron. Soc. **160**, 99 (1972).
[41] Y. Itikawa, R. Srivastava, and K. Sakimoto, Phys. Rev. A **44**, 7195 (1991).
[42] F. Bely Dubau, J. Dubau, P. Faucher, and A. H. Gabriel, Mon. Not. R. Astron. Soc. **198**, 239 (1982).
[43] A. A. Radzig and B. M. Smirnov, *Reference Data on Atoms, Molecules, and Ions,* Springer Series in Chemical

Physics Vol. 31 (Springer-Verlag, Berlin, 1985).
[44] K. Blum, *Physics of Atoms and Molecules* (Plenum, New York, 1981).
[45] P. J. Mohr, *Beam-Foil Spectroscopy,* edited by I. A. Sellin and D. J. Pegg (Plenum, New York, 1976), Vol. 1, p. 97.
[46] G. W. F. Drake, Can. J. Phys. **66**, 586 (1988).
[47] J. Dubau, M. Cornille, and F. Bely Dubau, in *Flare Physics in Solar Activity Maximum 22,* edited by Yutaca Uchida, Richard C. Canfield, Eijiro Hiei, and Tetsuya Watanabe, Springer Lecture Notes in Physics Vol. 387 (Springer-Verlag, Berlin, 1991), p. 141.
[48] M. Chaker, J. C. Kieffer, J. P. Matte, H. Pépin, P. Audebert, P. Maine, D. Strickland, P. Bado, and G. Mourou, Phys. Fluids B **3**, 167 (1991).
[49] J. C. Kieffer, M. Chaker, J. P. Matte, H. Pépin, C. Y. Côté, Y. Beaudoin, T. W. Johnston, C. Y. Chien, S. Coe, G. Mourou, and O. Peyrusse, Phys. Fluids B **5**, 2676 (1993).
[50] J. C. Kieffer, M. Chaker, J. P. Matte, C. Y. Côté, Y. Beaudoin, Z. Jiang, C. Y. Chien, S. Coe, G. Mourou, O. Peyrusse, and D. Gilles, in *Short Pulse High Intensity Lasers and Applications II,* edited by H. Baldis, SPIE Proc. Vol. 1860 (SPIE, Bellingham, WA, 1993), p 127.
[51] P. Maine, D. Strickland, P. Bado, M. Pesot, and G. Mourou, IEEE J. Quantum Electron. **24**, 398 (1988).
[52] J. C. Kieffer, P. Audebert, M. Chaker, J. P. Matte, H. Pépin, P. Maine, D. Meyerhofer, J. Delettrez, D. Strickland, P. Bado, and G. Mourou, Phys. Rev. Lett. **62**, 760 (1989).
[53] J. C. Kieffer, J. P. Matte, S. Béliar, M. Chaker, P. Audebert, H. Pépin, P. Maine, D. Strickland, P. Bado, and G. Mourou, IEEE J. Quantum Electron. **25**, 2640 (1989).
[54] Y. Beaudoin, C. Y. Chien, S. Coe, J. L. Tapié, and G. Mourou, Opt. Lett. **17**, 865 (1992).
[55] J. C. Kieffer *et al.*, in *X-Ray Laser 92,* IOP Conf. Proc. No. 125 (Institute of Physics and Physical Society, London, 1992), Sec. 4, p. 201.
[56] J. C. Kieffer *et al.*, in *Proceedings on Short Wavelength Radiation,* edited by P. Corkum and M. Perry (Optical Society of America, Washington, DC, in press).
[57] J. C. Kieffer, M. Chaker, C. Y. Côté, Y. Beaudoin, C. Y. Chien, S. Coe, and G. Mourou, Appl. Opt. **32**, 247 (1993).
[58] P. Audebert, J. P. Geindre, J. C. Gauthier, A. Mysyrowics, J. P. Chambaret, and A. Antonetti, Europhys. Lett. **19**, 189 (1992).
[59] H. Chen, B. Soom, B. Yaakobi, S. Uchida, and D. D. Meyerhofer, Phys. Rev. Lett. **70**, 3431 (1993).
[60] C. Darrow, S. Lane, D. Klem, and M. D. Perry, in *Short Pulse High Intensity Lasers and Applications II* (Ref. [50]), p. 46.
[61] V. P. Silin and S. A. Uryupin, Zh. Eksp. Teor. Fiz. **98**, 117 (1990) [Sov. Phys. JETP **71**, 64 (1990)].
[62] P. Mora, Ph.D. thesis, Univ. Paris Sud, Orsay, 1980 (unpublished); P. Mora and R. Pellat, Phys. Fluids **22**, 2408 (1979).